

**Random sequential adsorption of lattice animals on a three-dimensional cubic lattice**I. Lončarević,<sup>1</sup> Lj. Budinski-Petković,<sup>1</sup> J. R. Šćepanović,<sup>2</sup> Z. M. Jakšić,<sup>2</sup> and S. B. Vrhovac<sup>2,\*</sup><sup>1</sup>*Faculty of Engineering, Trg D. Obradovića 6, Novi Sad 21000, Serbia*<sup>2</sup>*Scientific Computing Laboratory, Center for the Study of Complex Systems, Institute of Physics Belgrade, University of Belgrade, Pregrevica 118, Zemun 11080, Belgrade, Serbia*

(Received 15 September 2019; published 14 January 2020)

The properties of the random sequential adsorption of objects of various shapes on simple three-dimensional (3D) cubic lattice are studied numerically by means of Monte Carlo simulations. Depositing objects are “lattice animals,” made of a certain number of nearest-neighbor sites on a lattice. The aim of this work is to investigate the impact of the geometrical properties of the shapes on the jamming density  $\theta_j$  and on the temporal evolution of the coverage fraction  $\theta(t)$ . We analyzed all lattice animals of size  $n = 1, 2, 3, 4$ , and  $5$ . A significant number of objects of size  $n \geq 6$  were also used to confirm our findings. Approach of the coverage  $\theta(t)$  to the jamming limit  $\theta_j$  is found to be exponential,  $\theta_j - \theta(t) \sim \exp(-t/\sigma)$ , for all lattice animals. It was shown that the relaxation time  $\sigma$  increases with the number of different orientations  $m$  that lattice animals can take when placed on a cubic lattice. Orientations of the lattice animal deposited in two randomly chosen places on the lattice are different if one of them cannot be translated into the other. Our simulations performed for large collections of 3D objects confirmed that  $\sigma \cong m \in \{1, 3, 4, 6, 8, 12, 24\}$ . The presented results suggest that there is no correlation between the number of possible orientations  $m$  of the object and the corresponding values of the jamming density  $\theta_j$ . It was found that for sufficiently large objects, changing of the shape has considerably more influence on the jamming density than increasing of the object size.

DOI: [10.1103/PhysRevE.101.012119](https://doi.org/10.1103/PhysRevE.101.012119)**I. INTRODUCTION**

A broad variety of structures are created of objects packed together, and describing the packing processes are among the most persistent problems in science [1,2]. Understanding of various aspects of packing is of a great scientific and industrial importance, with applications in nanotechnology, material science, biology, agriculture, and ecology [3–7]. Particle packing is still far from well understood. Packing structure is still not able to be predicted by a general model that takes into account various controlling parameters, such as geometric and material properties of objects, gravity, and packing methods.

One common approach to studying the packaging of objects of various shapes is the random sequential adsorption (RSA) method [8] which appears to be the simplest but non-trivial model of random packing. The RSA model considers sequential addition of particles of various shapes at randomly chosen places on the  $n$ -dimensional substrate. Overlapping of the particles is not allowed, and there is no diffusion of the deposited objects. The time evolution of the coverage (or the density of the system),  $\theta(t)$ , i.e., the fraction of the substrate occupied by the deposited objects at time  $t$ , describes the kinetic properties of the deposition process. Once an object is placed, it affects the geometry of all later placements, so that the dominant effect in RSA is the blocking of the available substrate space. At sufficiently large times the coverage  $\theta(t)$  approaches the jamming value  $\theta_j$ , where only gaps too small to place new particles are left on the substrate.

Depending on the system of interest, the substrate can be continuum or discrete, and RSA models can differ in substrate dimensionality. Analytical results are available mostly for one-dimensional problems [9–11]. Due to the complexity of deposition of objects of various shapes in higher dimensions, Monte Carlo simulations remain a main tool for describing such systems. The long-term behavior of the coverage fraction  $\theta(t)$  is known to be asymptotically algebraic for continuum substrates [11–15] and exponential for lattice models [16–20]. For the discrete case, the approach of the density  $\theta(t)$  to the jamming limit  $\theta_j$  is of the form

$$\theta_j - \theta(t) \sim \exp(-t/\sigma), \quad (1)$$

where jamming density  $\theta_j$  and the characteristic time  $\sigma$  are the parameters that depend on the details of the model, such as shape and symmetry properties of the depositing objects [17,18,20]. In our model, relaxation time  $\sigma$  is the fitting parameter that will be discussed within the context of the orientational freedom of the shape.

During the past few decades the methods of random sequential deposition of different objects on substrates of various dimensions have developed extensively. Previously, the majority of work has been done for spherical particles [21–23]. To examine the significance of particle anisotropy in formation of the jammed state coverings, RSA of many different object shapes has been studied for both continuum and lattice models. For example, RSA on continuous substrates has been studied for lines and ellipses [24,25], rectangles [26,27], starlike particles [28], superdisks bounded by the Lamé curves [29], spherocylinders and ellipsoids [24,30], cubes [31], cuboids [32], and polymers modeled as chains

\*vrhovac@ipb.ac.rs; <http://www.ipb.ac.rs/~vrhovac/>

of identical spheres [33]. It was found that the kinetics of irreversible deposition and morphological characteristics of the packing are strongly dependent on the shape and size of the depositing particles.

Formation of random deposits on discrete substrates has also been extensively studied for various object shapes [16–19,34,35]. Wang and Pandey [36] have studied the RSA kinetics of self-avoiding walk chains on a square lattice and found that the jamming coverage decreases with the chain length according to a power law. Deposition of objects of various sizes and rotational symmetries was studied for a square and triangular lattice [17,18]. It was found that the rapidity of the approach to the jamming coverage depends only on the symmetry order of the shape. The crucial role of the object shape in deposition dynamics was also confirmed in Ref. [20], where the depositing objects were formed by self-avoiding lattice steps, whereby the size of the objects was gradually increased by wrapping the walks in several different ways. Values of the relaxation time  $\sigma$  have been found to depend only on the symmetry properties of the shape, and it can be seen that objects differing in only one lattice step can have significantly different values of the relaxation time. This work provides the link between the decay of probability for the insertion of a new particle onto a lattice and the intrinsic properties of the shapes, such as parameter of nonsphericity of the objects.

Much attention has been paid to the RSA on 1D and 2D lattices, but there are only a few studies of irreversible deposition in 3D. Irreversible deposition on three-dimensional lattices has been studied mostly for  $k$ -mers [37–40]. Tarasevich and Cherkasova [38] examined the percolation and jamming properties of dimers on simple 3D cubic lattices. In Ref. [40], the study of Tarasevich and Cherkasova is extended to larger  $k$ -mers ( $2 \leq k \leq 64$ ) to determine the dependence of the jamming coverage on the size of the deposited  $k$ -mers for 3D cubic lattices. To the best of our knowledge, there are no results for RSA of various shapes formed by connected sites on a 3D lattice. It should be stressed that examining all possible positions of irregular shapes during the RSA process is complex and very time consuming. There is also a number of papers dealing with percolations in 3D [41–45], including some results for more complex systems.

It is obvious that object deposition is not physically realizable in three dimensions since sometimes it requires objects to be placed in locations that are surrounded by objects previously deposited. However, RSA in 3D is useful as the simplest, yet nontrivial model of random packing, which takes into account excluded volume effects. Most research is focused on the random close packings (RCPs) where neighboring particles touch each other [2]. The RCP state is difficult to define because by introducing order, higher packing fractions can be obtained [46]. In other words, the properties of RCPs are very sensitive to a numerical protocol used for packing objects. In contrast to random close packings, for RSA packing, the mean packing density is unambiguously defined, and it is more convenient for studying the influence of object shape on the structure of the packing and its density.

The aim of this work is to study the RSA of large collections of objects made by connected sites on a simple 3D cubic lattice, the so called “lattice animals.” More precisely, a lattice

animal can be viewed as a finite set of lattice sites connected by a network of nearest neighbor bonds. Object size is the number  $n$  of nodes that lattice animal covers on the grid. In the physics literature lattice animals are often called clusters, due to their close relationship to percolation problems [47,48]. Series expansions for the percolation probability or the average cluster size can be obtained as weighted sums over the number of lattice animals  $g_{n,p}$ , enumerated according to their size  $n$  and perimeter  $p$  [49]. Lattice animals have also been suggested as a model of branched polymers with excluded volume [50,51]. In the present study the deposition kinetics and the jamming limit are analyzed for all lattice animals of size  $n = 1, 2, 3, 4$ , and 5 (41 different shapes). Our results suggest that the number of different orientations that lattice animals can take when placed on a cubic lattice exerts a decisive influence on the adsorption kinetics near the jamming limit  $\theta_j$ . To further confirm this finding, we have analyzed some additional lattice animals of size  $n = 6$  (8 objects) and  $n \geq 7$  (11 objects).

The paper is organized as follows. Section II describes the model and the details of the simulations. The jamming densities and the jamming configurations are analyzed in Sec. III A. The approach of the coverage fraction  $\theta(t)$  to the jamming limit  $\theta_j$  is analyzed in Sec. III B. Finally, Sec. IV contains some additional comments.

## II. DEFINITION OF THE MODEL AND THE SIMULATION METHOD

Depositing objects are “lattice animals,” made of a certain number of connected sites. In mathematics, and combinatorics in particular, the term polyominoes and polycubes are frequently used for 3D discrete objects. A polyomino of size  $n$  is an edge-connected set of  $n$  squares on the square lattice  $\mathcal{Z}^2$  (the set of integers is denoted by  $\mathcal{Z}$ ). Polycubes are the 3D analogues of the planar polyominoes, i.e., polycube of size  $n$  is a face-connected set of  $n$  cubes in the simple-cubic lattice  $\mathcal{Z}^3$ . Because the square (cubic) lattice is self-dual, the number of polyominoes (polycubes) with  $n$  cells is precisely the number of 2D (3D) site animals with  $n$  vertices. Consequently, polyominoes (polycubes) are equivalent to site animals on the dual lattice. In this work we use the term “lattice animal” interchangeably with the other relevant terms such as “polyomino” and “polycube.”

Fixed polycubes are considered distinct if they have different shapes or orientations. In other words, two fixed polycubes are identical if one of them can be translated into the other. The number of fixed  $d$ -dimensional polycubes of size  $n$  is usually denoted in the literature by  $A_d(n)$ . In the mathematical literature, fixed polycubes are most discussed in the context of simple combinatorial problem—enumeration. Enumeration deals with determining the number of polycubes corresponding to a certain parameter, usually their size or perimeter. Lunnon [52] has made the first successful enumeration. He computed the number of polyominoes up to size 18 [with a slight error in  $A_2(17)$ ]. It is very interesting that to this day there is no known analytic formula for  $A_d(n)$  ( $d > 1$ ). The only known methods for computing  $A_d(n)$  are based on explicitly or implicitly enumerating all the polyominoes or polycubes using various numerical algorithms [52–56].

TABLE I. All polycubes (x) of size  $n = 1, 2, 3, 4$  and their number of orientations  $m$ .

(x)	$m$	shape	(x)	$m$	shape
(M)	1		(I4)	3	
(D)	3		(L4)	24	
(I3)	3		(O4)	3	
(V3)	12		(P4)	8	
(A4)	12		(S4)	12	
(B4)	12		(T4)	12	

Free lattice animals, however, are distinguished only by shape, not by orientation. The number of free  $d$ -dimensional polycubes of size  $n$  with  $m$  different orientations is denoted by  $A_d^m(n)$ . Lunnon [57] analyzed three-dimensional polycubes by considering symmetry groups, and computed (manually!)  $A_3(n)$  up to  $n = 6$ . Most polycubes are asymmetric, but many have more complex symmetry groups. The maximum symmetry for a polycube is the full symmetric group of a cube, with 48 elements—achiral octahedral group  $O_h$ . Lunnon found [57] that  $O_h$  has 98 subgroups falling into 33 conjugacy sets (polycube symmetry types). A polycube without symmetry has 24 different orientations. This is easy to visualize with a die. A die has 6 faces numbered 1 thru 6. If we place a die on the table with the “1” showing up, then we can rotate it to get 4 different orientations with the “1” still on top. Since there are 6 faces, there are  $6 \times 4 = 24$  different orientations. It is evident that a number of orientations that a polycube may take varies with the symmetry of the polycube. Since we solely consider free lattice animals in this work, the term “free” is omitted in the following text.

Table I shows all polycubes of size  $n = 1, 2, 3,$  and  $4$ . Polycubes of size  $n = 1, 2, 3$  are planar with a maximum of 12 different orientations (object V3). There are eight tetracubes

TABLE II. All polycubes (x) of size  $n = 5$  and their number of orientations  $m$ .

(x)	$m$	shape	(x)	$m$	shape	(x)	$m$	shape	(x)	$m$	shape
(A5)	24		(L25)	24		(S15)	24		(V25)	12	
(F5)	24		(L35)	24		(S25)	24		(W5)	12	
(I5)	3		(L45)	24		(T5)	12		(X5)	3	
(J15)	12		(N5)	24		(T15)	12		(Y5)	24	
(J25)	24		(N15)	24		(T25)	24		(Z5)	12	
(J45)	24		(N25)	24		(U5)	12				
(L5)	24		(P5)	24		(V5)	12				
(L15)	12		(Q5)	24		(V15)	12				

TABLE III. Some polycubes (x) of size  $n = 6$  and their number of orientations  $m$ .

(x)	$m$	shape
(I06)	3	
(Ba6)	4	
(Xb6)	6	
(Tp6)	6	
(Th6)	12	
(Zf6)	12	
(Te6)	24	
(Ti6)	24	

(fourth-order polycubes), five of which are planar [58]. It must be emphasized that polycubes are usually counted with mirror pairs (so-called chiral twins) distinguished, as would be natural for the cubical case in ordinary space. For example, a tetracube A4 and its mirror image B4 are considered distinct because there is no rigid motion that transforms one onto the other.

All polycubes of size  $n = 5$  (pentacubes) are shown in Table II. There are 29 distinct three-dimensional pentacubes [58]. As it can be seen, 12 pentacubes are flat and correspond to solid *pentominoes*. Among the nonplanar pentacubes, there are five that have at least one plane of symmetry (A5, L35, Q5, T15, T25) and each of them is its own mirror image. The remaining twelve nonplanar pentacubes form six chiral pairs: {J15, L15}, {J25, L25}, {J45, L45}, {N15, S15}, {N25, S25}, {V15, V25}. Of the 29 pentacubes, for two flats (I5, X5) there are only three possible orientations. Ten pentacubes have twelve orientations and each of the remaining 17 pentacubes has 24 orientations.

Polycubes of size  $n \leq 5$  can have 1, 3, 8, 12, or 24 different orientations. However, there are hexacubes (sixth-order polycubes) that have four and six different orientation. There are 166 hexacubes, 35 of which are planar [58]. Some hexacubes are shown in Table III. Hexacube Ba6 is the sole polycube of size  $n \leq 6$  with four orientations. It is interesting that among the polycubes of size  $n \leq 6$  only one object has eight different orientations (see, tetracube P4 in Table I).

TABLE IV. Shown here is the number of polycubes  $A_3^m(n)$  of size  $n$  with the specified number of possible orientations  $m$ . The results are shown for all polycubes of size  $n \leq 6$ .

$n$	$A_3^1$	$A_3^3$	$A_3^4$	$A_3^6$	$A_3^8$	$A_3^{12}$	$A_3^{24}$	$N = \sum_m A_3^m$
1	1							1
2		1						1
3		1				1		2
4		2			1	4	1	8
5		2				10	17	29
6		1	1	3		34	127	166

Further, three hexacubes have six orientations. Most of the hexacubes have 12 and 24 different orientations (34 and 127 objects, respectively). Table IV shows the number of possible orientations  $m$  for polycubes of size  $n \leq 6$  and the number of objects  $A_3^m(n)$  with the specified number of orientations.

### A. Simulation method

In this paper the *primary* lattice animal is a connected set of sites in  $\mathbb{Z}^3$  that contains the origin (0,0,0). We call that point the head of an object. At each Monte Carlo step a lattice site is selected at random. If the selected site is unoccupied, then deposition of the object is tried in one of the 24 orientations which is chosen at random. Then we fix the head of the object at the selected site and search whether all necessary sites are unoccupied. If so, then we occupy these sites and place the object. If the attempt fails, then a new site and a new orientation are selected at random, and so on.

It is crucial to explain how to choose a random object orientation. A basic rotation of the lattice animal is a rotation about one of the axes of a coordinate system. Each rotation is specified by an angle  $\psi$  of rotation. The rotation angle  $\psi$  is defined to be positive for a rotation that is counterclockwise when viewed by an observer looking along the rotation axis towards the origin. In accordance with the Euler's rotation theorem any arbitrary rotation can be composed of a combination of these three rotations [59]. The rotation matrices that rotate a vector around the  $x$ ,  $y$ , and  $z$  axes are given by [59]

$$R_x(\alpha) = \begin{bmatrix} 1 & 0 & 0 \\ 0 & \cos(\psi_1) & -\sin(\psi_1) \\ 0 & \sin(\psi_1) & \cos(\psi_1) \end{bmatrix}$$

(counterclockwise rotation around  $x$  axis), (2)

$$R_y(\beta) = \begin{bmatrix} \cos(\psi_2) & 0 & \sin(\psi_2) \\ 0 & 1 & 0 \\ -\sin(\psi_2) & 0 & \cos(\psi_2) \end{bmatrix}$$

(counterclockwise rotation around  $y$  axis), (3)

$$R_z(\gamma) = \begin{bmatrix} \cos(\psi_3) & -\sin(\psi_3) & 0 \\ \sin(\psi_3) & \cos(\psi_3) & 0 \\ 0 & 0 & 1 \end{bmatrix}$$

(counterclockwise rotation around  $z$  axis). (4)

For example, a vector  $\mathbf{v}$  can be rotated in any direction using a composition of three rotations [59]:  $\mathbf{v}' = R_a(\psi_1)R_b(\psi_2)R_c(\psi_3)\mathbf{v}$ ,  $a, b, c \in \{x, y, z\}$ . In our model, rotation angles can take the following values:  $\psi_1, \psi_2, \psi_3 \in \{0, \pi/2, \pi, 3\pi/2\}$ .

When choosing a random object orientation, it is essential that the numerical algorithm provides a search of all possible object orientations. If we apply a sequence  $R_a R_b R_c$ ,  $a, b, c \in \{x, y, z\}$  of basic 3D rotations to the lattice animal, then it is known that the order in which they are applied affects the final result. In other words, operators of rotation in 3D [Eq. (4)] are noncommutative [59]. Therefore, when we try to deposit an object, one random permutation  $(a b c)$  of

a set  $\{x, y, z\}$  is selected at first. Random permutation  $(a b c)$  defines the order of successive rotations  $R_a R_b R_c$  of an object about the axes  $a, b, c \in \{x, y, z\}$  of the coordinate system. Further, three random rotation angles  $\psi_1, \psi_2, \psi_3$  of an object around the  $a, b, c \in \{x, y, z\}$  axes are chosen from the set  $\{0, \pi/2, \pi, 3\pi/2\}$ . The primary object is rotated by applying the operator  $R_a(\psi_1)R_b(\psi_2)R_c(\psi_3)$ , after which its head is moved from the point  $(0,0,0)$  to a randomly selected lattice site and checked for any overlap with neighboring lattice animals already placed in the lattice. Let us remark that a different choice of the head of the object does not change the obtained results. We have verified that usage of different heads for all examined objects gives quantitatively the same results

TABLE V. All lattice animals (x) of size  $n = 1, 2, 3, 4$  and their number of orientations  $m$ .

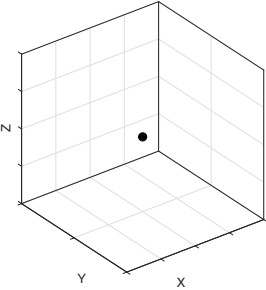
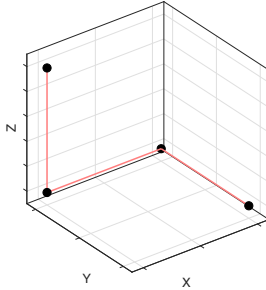
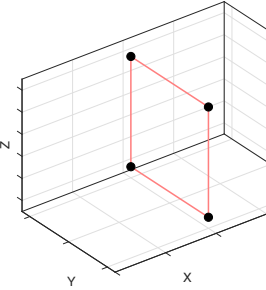
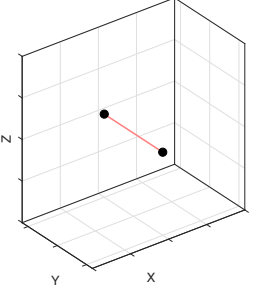
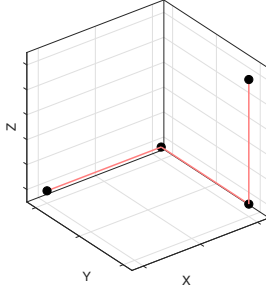
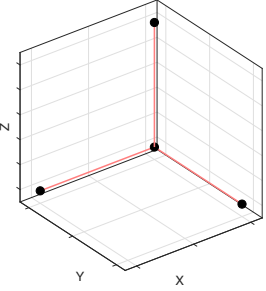
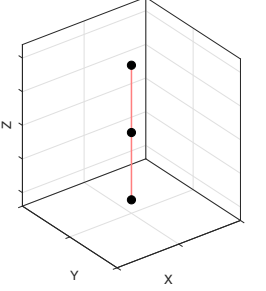
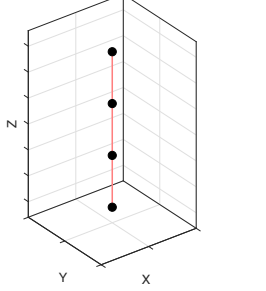
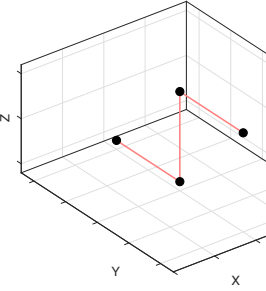
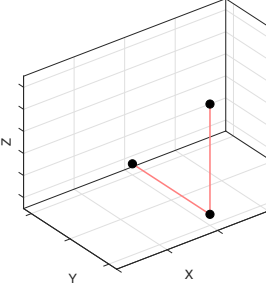
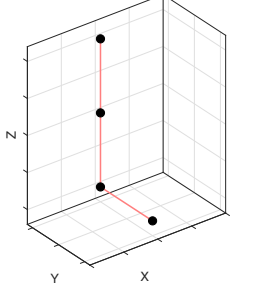
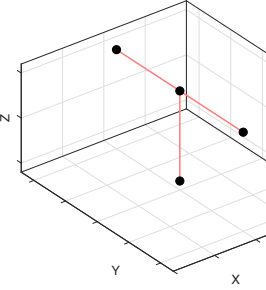
(x), $m$ shape	(x), $m$ shape	(x), $m$ shape
(M),1 	(A4),12 	(O4),3 
(D),3 	(B4),12 	(P4),8 
(I3),3 	(I4),3 	(S4),12 
(V3),12 	(L4),24 	(T4),12 

TABLE VI. All lattice animals (x) of size  $n = 5$  and their number of orientations  $m$ .

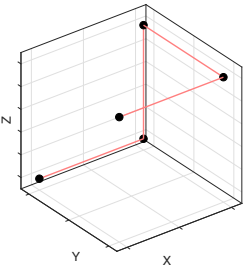
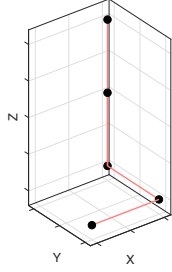
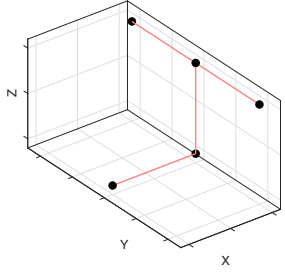
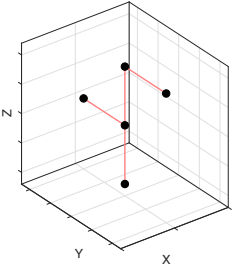
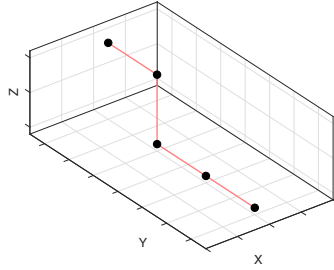
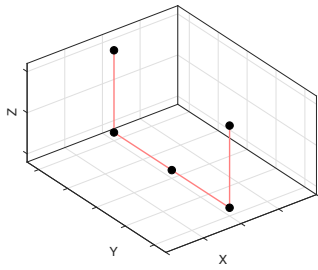
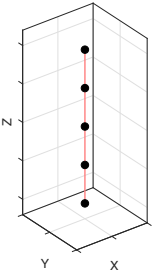
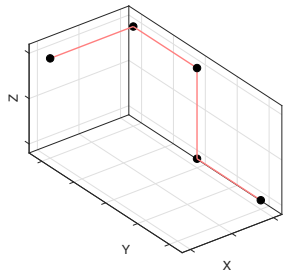
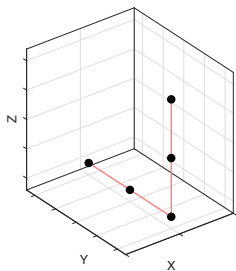
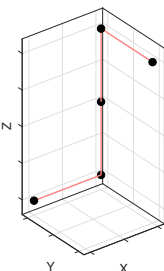
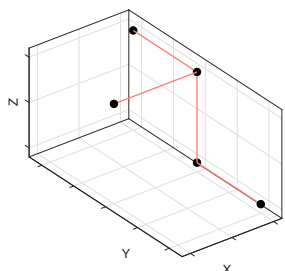
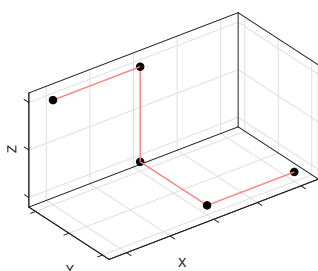
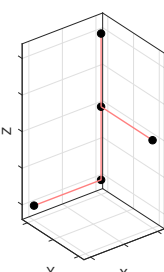
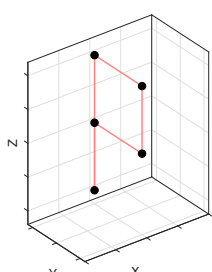
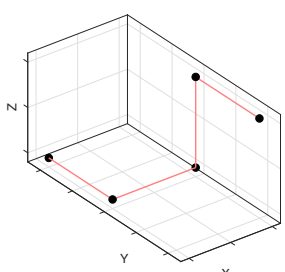
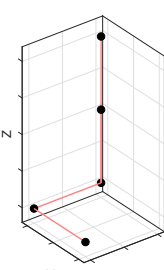
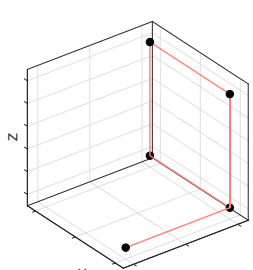
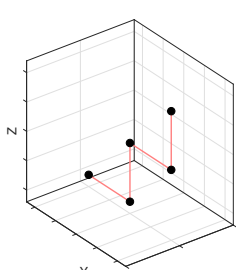
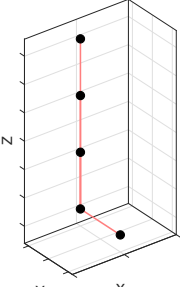
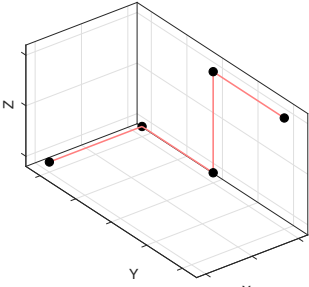
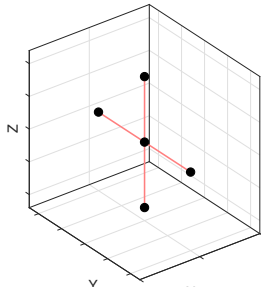
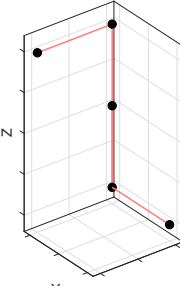
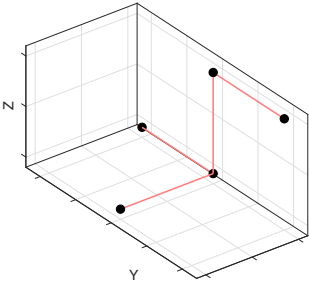
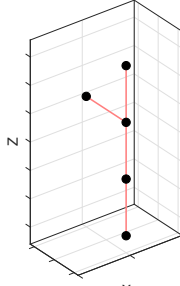
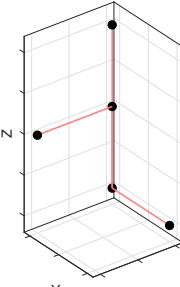
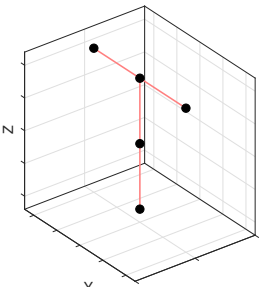
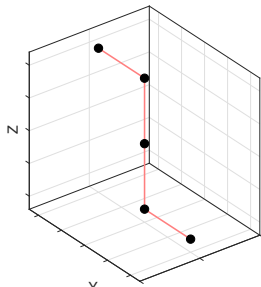
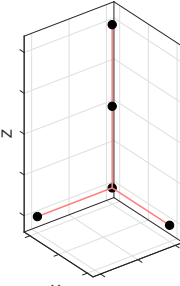
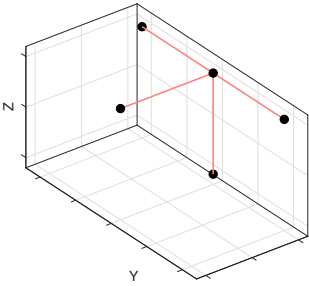
(x), $m$ shape	(x), $m$ shape	(x), $m$ shape
(A5),24 	(L45),24 	(T25),24 
(F5),24 	(N5),24 	(U5),12 
(I5),3 	(N15),24 	(V5),12 
(J15),12 	(N25),24 	(V15),12 
(J25),24 	(P5),24 	(V25),12 
(J45),24 	(Q5),24 	(W5),12 

TABLE VI. (Continued.)

(x), $m$ shape	(x), $m$ shape	(x), $m$ shape
 <p>(L5),24</p>	 <p>(S15),24</p>	 <p>(X5),3</p>
 <p>(L15),12</p>	 <p>(S25),24</p>	 <p>(Y5),24</p>
 <p>(L25),24</p>	 <p>(T5),12</p>	 <p>(Z5),12</p>
 <p>(L35),24</p>	 <p>(T15),12</p>	

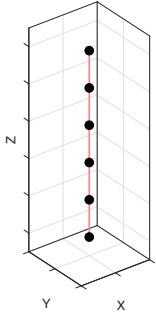
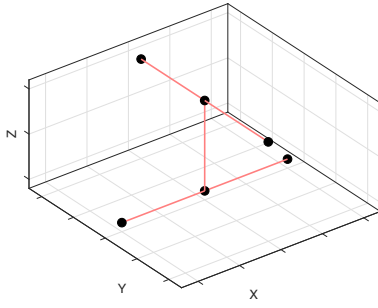
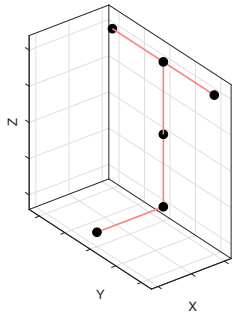
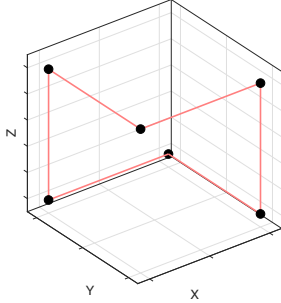
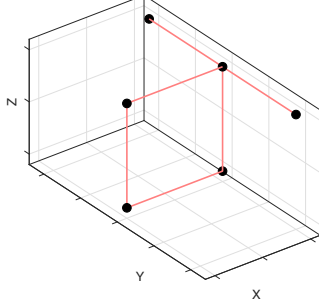
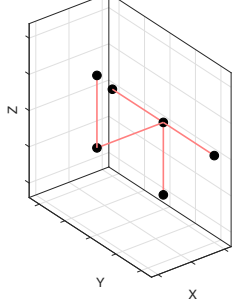
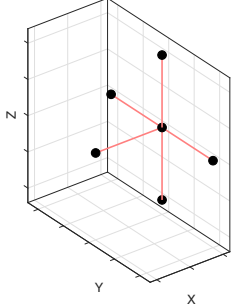
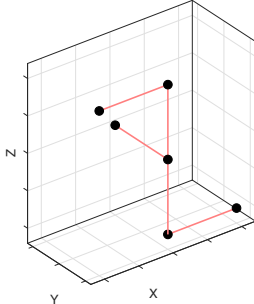
for the temporal evolution of density  $\theta(t)$  and the jamming limit  $\theta_j$ .

During the simulation, we can record the number of all inaccessible sites in the lattice. These include the occupied sites and the sites that are unoccupied but cannot be the head of the object deposited in any of the 24 possible orientations. The jamming limit is reached when the number of inaccessible sites is equal to the total number of sites in the lattice. Checking this condition is performed after every  $kL^2$  attempts to absorb the object, starting at some late time point estimated in the trial simulations on smaller

lattices. Depending on the object size, the values of parameter  $k$  are 5, 20, and 50. If the condition is true, then we stop the current run and continue with the next simulation run.

The Monte Carlo simulations are performed on a 3D cubic lattice of size  $L = 128$ . Periodic boundary conditions are used in all directions. The time is counted by the number of attempts to select a lattice site and scaled by the total number of lattice sites  $L^3 \approx 2$  million. The data are averaged over 100 independent runs for each of the investigated lattice animals.

TABLE VII. Some lattice animals (x) of size  $n = 6$  and their number of orientations  $m$ .

(x), $m$ shape	(x), $m$ shape	(x), $m$ shape
 <p>(I06),3</p>	 <p>(Tp6),6</p>	 <p>(Te6),24</p>
 <p>(Ba6),4</p>	 <p>(Th6),12</p>	 <p>(Ti6),24</p>
 <p>(Xb6),6</p>	 <p>(Zf6),12</p>	

### III. RESULTS AND DISCUSSION

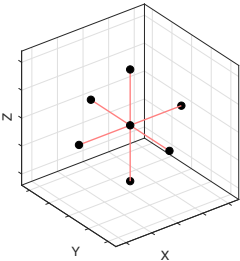
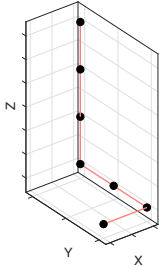
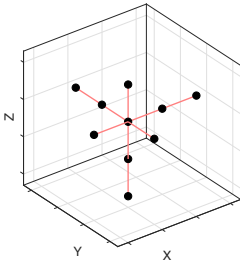
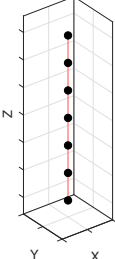
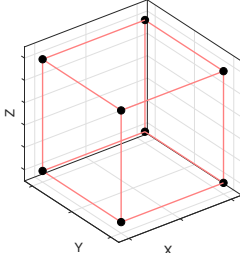
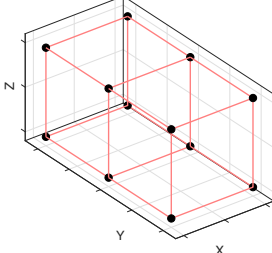
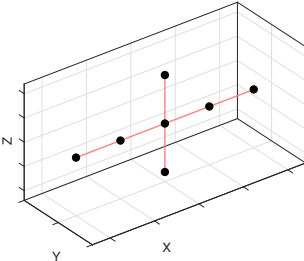
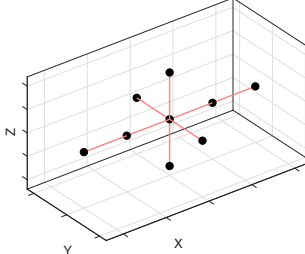
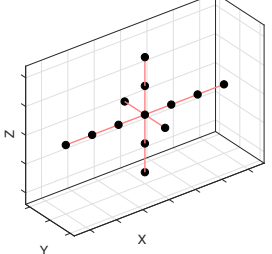
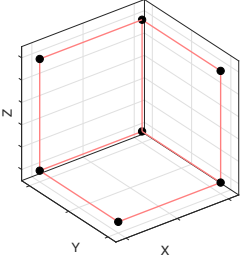
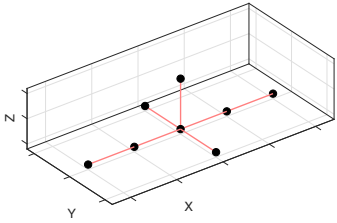
As stated in Sec. II, the structure of a polycube can be represented by means of a lattice animal that has a vertex for each cube and an edge for each two cubes that share a square. Lattice animals that are equivalent to polycubes presented in Tables I–III are shown in Tables V–VII. Some additional lattice animals of size  $n \geq 7$  are shown in Table VIII. The number of examined objects represents a good basis for studying the impact of the geometrical properties of the shapes on the packing process in 3D, i.e., on the jamming coverage  $\theta_j$  and on the temporal evolution of the coverage fraction  $\theta(t)$ .

#### A. Jamming densities

The first quantity of interest is the jamming limit  $\theta_j$  which is reached when no more objects can be placed in any position on the lattice. Numerical values of the obtained jamming limits  $\theta_j$  are given in Tables IX–XII for all examined shapes. We can see that in each chiral pair, both objects have the identical values of the jamming density. From Tables IX and X it is evident that for small shapes ( $n \leq 5$ ), jamming densities  $\theta_j$  decrease rapidly with the size  $n$  of the objects.

Most objects of size  $n \leq 4$  have a jamming density  $\theta_j$  greater than 0.80, while  $\theta_j$  for all objects of size  $n = 5$  is in the interval 0.70–0.80. Jamming densities  $\theta_j$  for all examined objects of size  $n \geq 7$  have values below  $\approx 0.70$ . Noticeable drop in the jamming density  $\theta_j$  is thus a clear consequence of the enhanced frustration of the spatial adsorption. However, adding a single node to large objects does not result in a significant increase in their size. Therefore, changing of the shape of the large objects has considerably more influence on the jamming density than increasing of the object size. For example, jamming densities for objects LA7b ( $n = 7$ ) and LA12 ( $n = 12$ ) with  $m = 3$  possible orientations from Table XII are almost identical  $\approx 0.67$ , although they are of different sizes. The results presented in Tables IX–XII also suggest that there is no correlation between the number of possible orientations of the object and the corresponding values of the jamming density  $\theta_j$ . Indeed, the jamming density of the object Xb6 with  $m = 6$  possible orientations is  $\theta_j \approx 0.68$ , but objects I06 and Ba6 with a smaller number of possible orientations than six have, respectively, a higher and lower  $\theta_j$  value than 0.68 (see Table XI). Similarly, the jamming density of the object LA7b with  $m = 3$  possible orientations is  $\theta_j \approx 0.67$ .

TABLE VIII. Some lattice animals ( $x$ ) of size  $n \geq 7$  and their number of orientations  $m$ .

$(x), m$ shape	$(x), m$ shape	$(x), m$ shape
 (LA7a),1	 (LA7e),24	 (LA10),8
 (LA7b),3	 (LA8a),1	 (LA12),3
 (LA7c),6	 (LA8b),3	 (LA13),6
 (LA7d),8	 (LA8c),12	

However, objects LA7c and LA7d with a greater number of possible orientations than three have, respectively, a lower and higher  $\theta_j$  value than 0.67 (see Table XII). Note that our results for the jamming densities of linear objects ( $k$ -mers: D, I3–I5, I06, LA7b) are in a good agreement with the results presented in reference [40] in which RSA of straight rigid rods on a simple cubic lattice is analyzed.

Figure 1 shows typical snapshot configurations at the jamming density obtained for objects (a) LA7a, (b) LA8b, (c) Ba6, (d) Xb6, (e) P4, (f) T15, and (g) LA7e. The snapshots of size  $\Delta L^3 = 10^3$  are taken from the central part of the lattice. Figure 1 displays configurations for seven objects that match all values of the number of possible orientations ( $m = 1, 3, 4, 6, 8, 12, 24$ ) for given objects.

### B. RSA kinetics

Now, we report and discuss the numerical results regarding the influence of the number of possible orientations of the

shape on the kinetics of the deposition processes. Figures 2–6 show the plots of  $\ln[\theta_j - \theta(t)]$  versus  $t$  for seven classes of the objects, i.e., for seven values  $m = 1, 3, 4, 6, 8, 12, 24$  of the number of different orientations that lattice animals can take when placed on a cubic lattice. Each of these figures contains results for objects with the same number of possible orientations. For all examined objects plots of  $\ln[\theta_j - \theta(t)]$  versus  $t$  are found to be straight lines at the late times of the deposition process, confirming the exponential approach to the jamming limit of the form Eq. (1), with parameters  $\sigma$  and  $\theta_j$  that depend on the shape of a depositing object. Furthermore, for a given value of  $m$ , these plots are parallel lines in the late stages of the deposition process for lattice animals of very different sizes [e.g., see Fig. 3(b)]. Hence, for objects that have the same value of the parameter  $m$ , rapidity of the approach to the jamming state is not affected by the size of the object. The number of possible orientations  $m$  of the object has an essential influence in the late times of the deposition process. Lines with

TABLE IX. For each lattice animal (x) of size  $n = 1, 2, 3, 4$  with  $m$  possible orientations,  $\theta_j^{(x)}$  is the jamming coverage and  $\sigma$  is the relaxation time [Eq. (1)]. The numbers in parentheses are the numerical values of the standard uncertainty of  $\theta_j^{(x)}$  referred to the last digits of the quoted value.

Shape (x), size $n$	$m$	$\sigma$	$\theta_j^{(x)}$
(M), $n = 1$	1	0.99	1.0000(0)
(D), $n = 2$	3	3.09	0.9184(1)
(I3), $n = 3$	3	3.16	0.8390(2)
(V3), $n = 3$	12	12.36	0.8788(2)
(A4), $n = 4$	12	12.45	0.8178(2)
(B4), $n = 4$	12	12.47	0.8178(2)
(I4), $n = 4$	3	3.19	0.7808(3)
(L4), $n = 4$	24	23.98	0.8339(2)
(O4), $n = 4$	3	3.06	0.8079(3)
(P4), $n = 4$	8	8.03	0.7941(3)
(S4), $n = 4$	12	12.08	0.8149(2)
(T4), $n = 4$	12	12.49	0.8114(3)

seven different slopes are plotted in Fig. 7, showing the late times of the deposition process corresponding to objects of

TABLE X. For each lattice animal (x) of size  $n = 5$  with  $m$  possible orientations,  $\theta_j^{(x)}$  is the jamming coverage and  $\sigma$  is the relaxation time [Eq. (1)]. The numbers in parentheses are the numerical values of the standard uncertainty of  $\theta_j^{(x)}$  referred to the last digits of the quoted value.

Shape (x)	$m$	$\sigma$	$\theta_j^{(x)}$
(A5)	24	24.21	0.7716(2)
(F5)	24	24.29	0.7860(3)
(I5)	3	3.18	0.7369(4)
(J15)	12	11.95	0.7635(2)
(J25)	24	24.72	0.7839(2)
(J45)	24	24.12	0.7958(3)
(L5)	24	23.91	0.7695(3)
(L15)	12	12.20	0.7635(3)
(L25)	24	24.24	0.7839(2)
(L35)	24	24.42	0.7774(3)
(L45)	24	24.88	0.7957(2)
(N5)	24	24.34	0.7866(3)
(N15)	24	24.88	0.7842(2)
(N25)	24	24.35	0.7790(3)
(P5)	24	24.20	0.8017(3)
(Q5)	24	23.95	0.7826(3)
(S15)	24	24.41	0.7841(2)
(S25)	24	24.25	0.7790(3)
(T5)	12	12.76	0.7500(3)
(T15)	12	12.43	0.7582(3)
(T25)	24	24.58	0.7863(2)
(U5)	12	12.48	0.7611(3)
(V5)	12	11.94	0.7628(3)
(V15)	12	12.37	0.7647(3)
(V25)	12	12.64	0.7647(3)
(W5)	12	12.31	0.7615(3)
(X5)	3	3.08	0.7007(3)
(Y5)	24	24.62	0.7595(3)
(Z5)	12	12.79	0.7643(2)

TABLE XI. For lattice animal (x) of size  $n = 6$  with  $m$  possible orientations,  $\theta_j^{(x)}$  is the jamming coverage and  $\sigma$  is the relaxation time [Eq. (1)]. The numbers in parentheses are the numerical values of the standard uncertainty of  $\theta_j^{(x)}$  referred to the last digits of the quoted value.

Shape (x)	$m$	$\sigma$	$\theta_j^{(x)}$
(I06)	3	3.06	0.7026(4)
(Ba6)	4	4.02	0.6683(3)
(Xb6)	6	6.03	0.6827(3)
(Tp6)	6	6.13	0.6879(4)
(Th6)	12	12.18	0.7179(3)
(Zf6)	12	12.25	0.7215(3)
(Te6)	24	24.55	0.7378(3)
(Ti6)	24	24.60	0.7369(3)

different number of possible orientations  $m$ , as indicated in the legend.

We have calculated the values of the parameter  $\sigma$  [Eq. (1)] from the slopes of the  $\ln[\theta_j - \theta(t)]$  versus  $t$  curves in the late times of the process. The parameter  $\sigma$  determines how fast the lattice is filled up to the jamming coverage  $\theta_j$ . The values of the relaxation time  $\sigma$  are given in Tables IX–XII for all examined lattice animals. Approximate values of the parameter  $\sigma$  for the seven classes of objects are found to be equal the number of possible orientations of the shape:

$$\sigma \simeq m \in \{1, 3, 4, 6, 8, 12, 24\}. \quad (5)$$

This means that the approach to the jamming limit is slower for objects with a larger number of possible orientations. At large times, adsorption events take place on islands of unoccupied sites. The individual islands act as selective targets for specific deposition events. In other words, there is only a restricted number of possible orientations in which an object can reach a vacant location, provided the location is small enough. Such difficult placement of an object in locations that allow only a small number of object orientations is a feature of the deposits near the jamming state. Namely, for an object

TABLE XII. For lattice animal (x) of size  $n \geq 7$  with  $m$  possible orientations,  $\theta_j^{(x)}$  is the jamming coverage and  $\sigma$  is the relaxation time [Eq. (1)]. The numbers in parentheses are the numerical values of the standard uncertainty of  $\theta_j^{(x)}$  referred to the last digits of the quoted value.

Shape (x), size $n$	$m$	$\sigma$	$\theta_j^{(x)}$
(LA7a), $n = 7$	1	0.98	0.6225(4)
(LA7b), $n = 7$	3	2.97	0.6749(5)
(LA7c), $n = 7$	6	6.19	0.6336(4)
(LA7d), $n = 7$	8	8.06	0.6897(4)
(LA7e), $n = 7$	24	24.20	0.7006(3)
(LA8a), $n = 8$	1	0.98	0.6453(5)
(LA8b), $n = 8$	3	3.11	0.5858(4)
(LA8c), $n = 8$	12	12.18	0.6308(3)
(LA10), $n = 10$	8	8.08	0.5693(4)
(LA12), $n = 12$	3	3.04	0.6719(5)
(LA13), $n = 13$	6	6.12	0.4899(4)

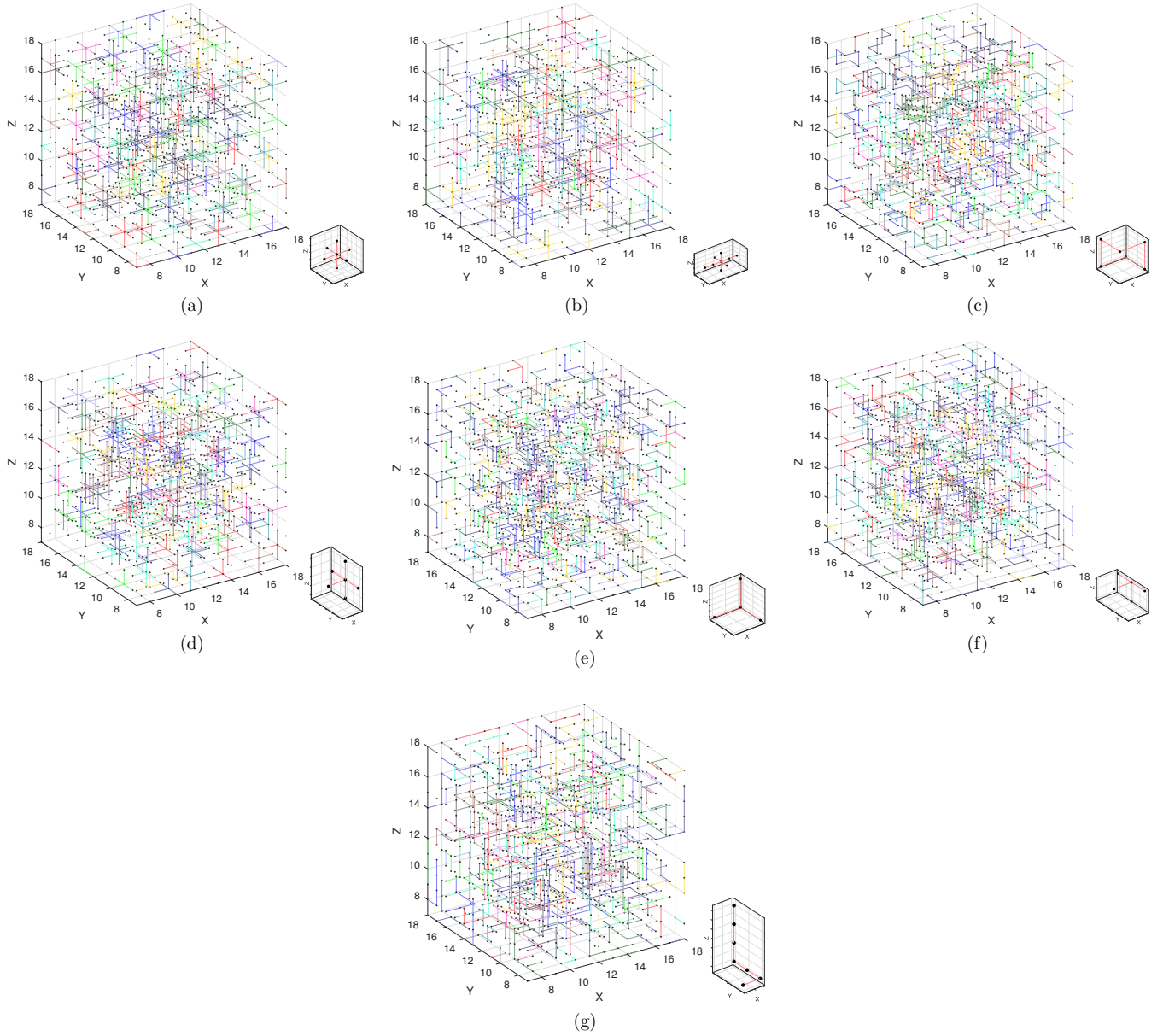


FIG. 1. Snapshots of patterns formed during the RSA of objects (a) LA7a,  $m = 1$  (Tables VIII and XII), (b) LA8b,  $m = 3$  (Tables VIII and XII), (c) Ba6,  $m = 4$  (Tables VII and XI), (d) Xb6,  $m = 6$  (Tables VII and XI), (e) P4,  $m = 8$  (Tables V and IX), (f) T15,  $m = 12$  (Tables VI and X), and (g) LA7e,  $m = 24$  (Tables VIII and XII). The snapshots are taken from the central part of the lattice at times needed for the system to reach the jamming state. A corresponding lattice animal is shown in the lower right corner of each panel (a)–(g). The objects are colored with 12 colors randomly selected for each one.

with a larger number of possible placements, a longer time is needed to examine all isolated empty locations that are left in the late times of the process. Hence, the increase in the number of possible placements of the shape reduces the rate of single particle adsorption. This extends the mean waiting time between consecutive and successful deposition events, and the approach to the jamming state is slower.

#### IV. CONCLUDING REMARKS

In the case of irreversible deposition on planar lattices, it is well established that the kinetics of the late stage of deposition is determined exclusively with the symmetry properties of the

shapes. For the shapes made by self-avoiding lattice steps on the 2D triangular lattice, relaxation time  $\sigma$  [Eq. (1)] is inversely proportional to the order of symmetry axis  $n_s$  of the shape,  $\sigma = 6/n_s$  [18,20]. However, for a planar shape with symmetry order  $n_s$  on a triangular lattice, the number of possible orientations is given exactly by the expression  $6/n_n$ . To generalise this result to 3D shapes, we have performed extensive numerical simulations of the RSA using large collections of objects (“lattice animals”) made by connected sites on a simple 3D cubic lattice.

As expected, the approach to the jamming limit  $\theta_j$  was found to be exponential for all the lattice animals. It was shown that the relaxation time  $\sigma$  [Eq. (1)] is equal to the

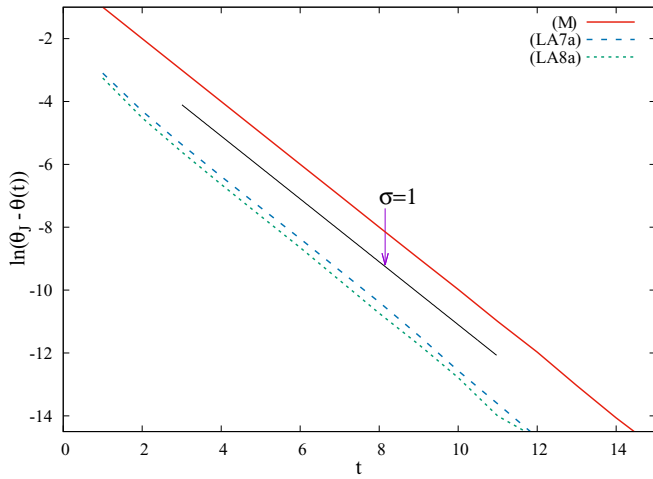


FIG. 2. Plots of  $\ln[\theta_j - \theta(t)]$  versus  $t$  for objects (M), (LA7a), and (LA8a) with one possible placement (Tables V and VIII). Additionally, the slanted straight line with the slope  $-1/\sigma = -1$  is shown, indicating the late-time RSA behavior and is guide to the eye.

number of different orientations  $m$  that lattice animals can take when placed on a cubic lattice [Eq. (5)]. To confirm this finding, we have analyzed all lattice animals of size  $n = 1, 2, 3, 4,$  and  $5$  (41 different shapes), eight lattice animals of size  $n = 6$  and eleven objects of size  $n \geq 7$ . In other words, the coverage kinetics is slowed down with the increase in the number of possible placements  $m$  of the shape. Indeed, the mean waiting time between consecutive deposition events

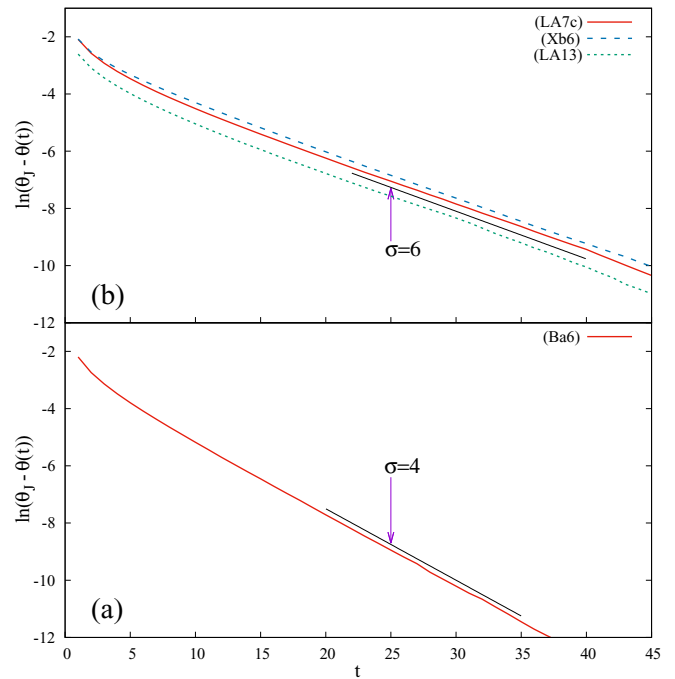


FIG. 4. Plots of  $\ln[\theta_j - \theta(t)]$  versus  $t$  for: (a) object (Ba6) with four possible placements (Table VII); (b) objects (LA7c), (Xb6), and (LA13) with six possible placements (Tables VII and VIII). Additionally, the slanted straight lines with the slopes  $-1/\sigma = -1/4$  (a),  $-1/6$  (b) are shown, indicating the late-time RSA behavior and are guide to the eye.

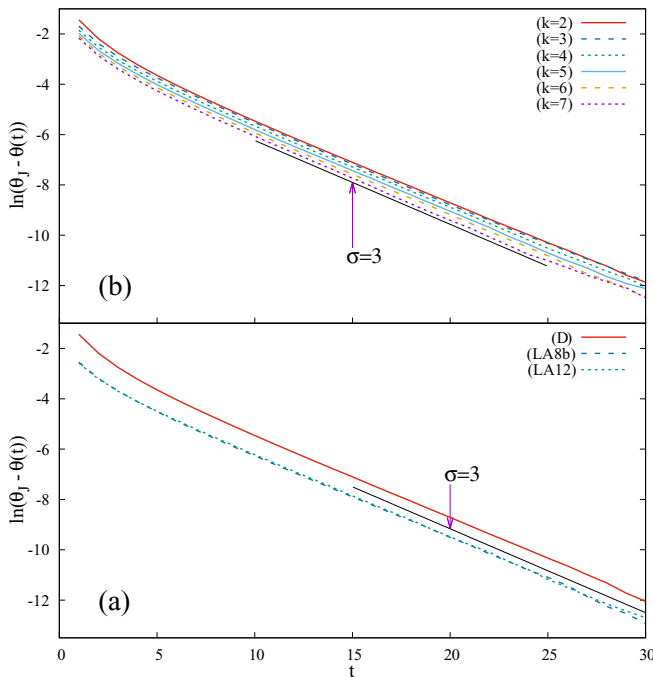


FIG. 3. Plots of  $\ln[\theta_j - \theta(t)]$  versus  $t$  for: (a) objects (D), (LA8b), and (LA12) with three possible placements (Tables V and VIII); (b)  $k$ -mers ( $k = 2, 3, 4, 5, 6, 7$ ). Additionally, the slanted straight lines with the slope  $-1/\sigma = -1/3$  are shown, indicating the late-time RSA behavior and are guide to the eye.

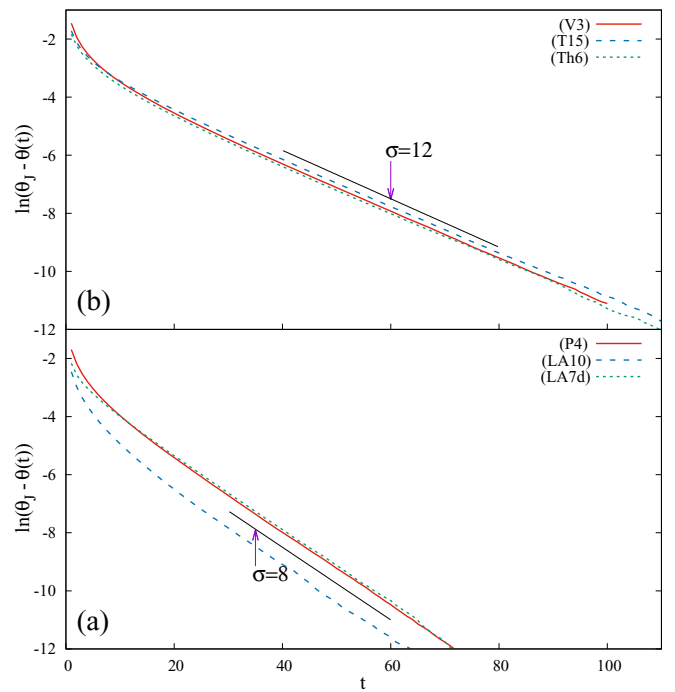


FIG. 5. Plots of  $\ln[\theta_j - \theta(t)]$  versus  $t$  for: (a) objects (P4), (LA10), and (LA7d) with eight possible placements (Tables V and VIII); (b) objects (V3), (T15), and (Th6) with 12 possible placements (Tables V, VI, and VII). Additionally, the slanted straight lines with the slopes  $-1/\sigma = -1/8$  (a),  $-1/12$  (b) are shown, indicating the late-time RSA behavior and are guide to the eye.

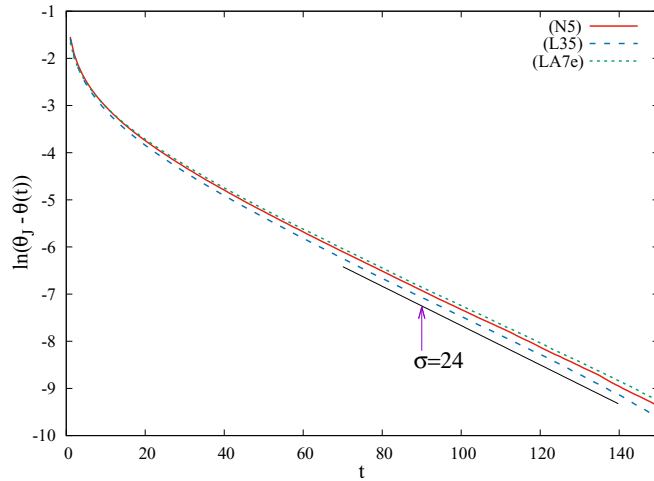


FIG. 6. Plots of  $\ln[\theta_j - \theta(t)]$  versus  $t$  for objects (N5), (L35), and (LA7e) with 24 possible placements (Tables VI and VIII). Additionally, the slanted straight line with the slope  $-1/\sigma = -1/24$  is shown, indicating the late-time RSA behavior and is guide to the eye.

extends with  $m$ , so that the approach to the jamming state is slower.

We have pointed out that for sufficiently large objects, changing of the shape has considerably more influence on the jamming density than increasing of the object size. These findings are in an excellent qualitative agreement with the results of Karayiannis and Laso [60,61]. They proposed a Monte Carlo scheme which is able to efficiently sample freely-jointed chains of hard spheres even up to the maximally random jammed (MRJ) state. In this model, chain connectivity imposes constraints that force bonded spheres to adopt specific local configurations. As an interesting result, the constraints imposed by chain connectivity were found to play a more important role in determining the MRJ states than the size of flexible chains. However, our results suggest that there is no correlation between the number of possible orientations of the object and the corresponding values of the jamming density  $\theta_j$ . In Ref. [20], special attention is paid to the behavior of probability  $p_{\text{insert}}$  for the insertion of a new particle onto a planar triangular lattice during the deposition process. Shape factor, defined as the degree to which a particle is similar to

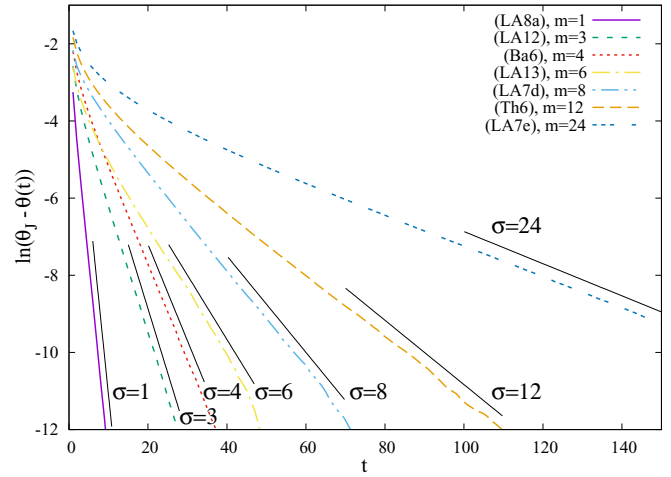


FIG. 7. Plots of  $\ln[\theta_j - \theta(t)]$  versus  $t$  for objects (LA8a), (LA12), (Ba6), (LA13), (LA7d), (Th6), and (LA7e) from Tables VII and VIII. The curves correspond to objects with the various number of possible orientations,  $m$ , as indicated in the legend. Additionally, the slanted straight lines with the slope  $-1/\sigma = -1, -1/3, -1/4, -1/6, -1/8, -1/12, -1/24$  are shown, indicating the late-time RSA behavior and are guides to the eye.

a circle, is associated with the evolution of probability  $p_{\text{insert}}$ . It would be interesting to perform a similar investigation with 3D objects of various shapes within the context of the shape descriptors, such as aspect ratios, compactness of the object, smoothness of the perimeter, and the shape factor. As an open possibility for the future, we think that the three-dimensional model presented in this work can be generalized to mixtures of several kinds of 3D objects.

## ACKNOWLEDGMENTS

This work was supported by the Ministry of Education, Science, and Technological Development of the Republic of Serbia under Projects No. ON171017 and No. III45016, and by the European Commission under H2020 Project VI-SEEM, Grant No. 675121. Numerical simulations were run on the PARADOX supercomputing facility at the Scientific Computing Laboratory of the Institute of Physics Belgrade.

- 
- [1] T. Aste, Variations around disordered close packing, *J. Phys.: Condens. Matter* **17**, S2361 (2005).
  - [2] S. Torquato and F. H. Stillinger, Jammed hard-particle packings: From Kepler to Bernal and beyond, *Rev. Mod. Phys.* **82**, 2633 (2010).
  - [3] P. M. Chaikin and T. C. Lubensky, *Principles of Condensed Matter Physics* (Cambridge University Press, New York, 1995).
  - [4] A. Donev, I. Cisse, D. Sachs, E. A. Variano, F. H. Stillinger, R. Connelly, S. Torquato, and P. M. Chaikin, Improving the density of jammed disordered packings using ellipsoids, *Science* **303**, 990 (2004).
  - [5] A. Dabrowski, Adsorption—From theory to practice, *Adv. Colloid Interface Sci.* **93**, 135 (2001).
  - [6] V. Privman (ed.), *Colloids Surf., A* **165**, 1 (2000) (a collection of review articles).
  - [7] A. Cadilhe, N. A. M. Araújo, and V. Privman, Random sequential adsorption: From continuum to lattice and pre-patterned substrates, *J. Phys.: Condens. Matter* **19**, 065124 (2007).
  - [8] J. W. Evans, Random and cooperative sequential adsorption, *Rev. Mod. Phys.* **65**, 1281 (1993).
  - [9] E. Ben-Naim and P. L. Krapivsky, On irreversible deposition on disordered substrates, *J. Phys. A: Math. Gen.* **27**, 3575 (1994).

- [10] M. C. Bartelt and V. Privman, Kinetics of irreversible multilayer adsorption: One-dimensional models, *J. Chem. Phys.* **93**, 6820 (1990).
- [11] R. H. Swendsen, Dynamics of random sequential adsorption, *Phys. Rev. A* **24**, 504 (1981).
- [12] J. Feder, Random sequential adsorption, *J. Theor. Biol.* **87**, 237 (1980).
- [13] Y. Pomeau, Some asymptotic estimates in the random parking problem, *J. Phys. A: Math. Gen.* **13**, L193 (1980).
- [14] B. Bonnier, Random sequential adsorption of binary mixtures on a line, *Phys. Rev. E* **64**, 066111 (2001).
- [15] M. Cieřla and J. Barbasz, Random packing of regular polygons and star polygons on a flat two-dimensional surface, *Phys. Rev. E* **90**, 022402 (2014).
- [16] S. S. Manna and N. M. Švrakić, Random sequential adsorption: Line segments on the square lattice, *J. Phys. A: Math. Gen.* **24**, L671 (1991).
- [17] Lj. Budinski-Petković and U. Kozmidis-Luburić, Jamming configurations for irreversible deposition on a square lattice, *Physica A: Stat. Mech. Appl.* **236**, 211 (1997).
- [18] Lj. Budinski-Petković and U. Kozmidis-Luburić, Random sequential adsorption on a triangular lattice, *Phys. Rev. E* **56**, 6904 (1997).
- [19] Lj. Budinski-Petković, S. B. Vrhovac, and I. Lončarević, Random sequential adsorption of polydisperse mixtures on discrete substrates, *Phys. Rev. E* **78**, 061603 (2008).
- [20] Lj. Budinski-Petković, I. Lončarević, D. Dujak, A. Karač, J. R. Šćepanović, Z. M. Jakšić, and S. B. Vrhovac, Particle morphology effects in random sequential adsorption, *Phys. Rev. E* **95**, 022114 (2017).
- [21] D. W. Cooper, Random-sequential-packing simulations in three dimensions for spheres, *Phys. Rev. A* **38**, 522 (1988).
- [22] J. Talbot, P. Schaaf, and G. Tarjus, Random sequential addition of hard spheres, *Mol. Phys.* **72**, 1397 (1991).
- [23] S. Torquato, O. U. Uche, and F. H. Stillinger, Random sequential addition of hard spheres in high euclidean dimensions, *Phys. Rev. E* **74**, 061308 (2006).
- [24] J. D. Sherwood, Random sequential adsorption of lines and ellipses, *J. Phys. A: Math. Gen.* **23**, 2827 (1990).
- [25] M. Cieřla, G. Pajak, and R. M. Ziff, In a search for a shape maximizing packing fraction for two-dimensional random sequential adsorption, *J. Chem. Phys.* **145**, 044708 (2016).
- [26] R. D. Vigil and R. M. Ziff, Kinetics of random sequential adsorption of rectangles and line segments, *J. Chem. Phys.* **93**, 8270 (1990).
- [27] W. Kasperek, P. Kubala, and M. Cieřla, Random sequential adsorption of unoriented rectangles at saturation, *Phys. Rev. E* **98**, 063310 (2018).
- [28] M. Cieřla and P. Karbowiczek, Random sequential adsorption of starlike particles, *Phys. Rev. E* **91**, 042404 (2015).
- [29] B. N. Aleksić, N. M. Švrakić, and M. Belić, Kinetics of deposition of oriented superdisks, *Phys. Rev. E* **88**, 062112 (2013).
- [30] P. Viot, G. Tarjus, S. M. Ricci, and J. Talbot, Random sequential adsorption of anisotropic particles. I. Jamming limit and asymptotic behavior, *J. Chem. Phys.* **97**, 5212 (1992).
- [31] M. Cieřla and P. Kubala, Random sequential adsorption of cubes, *J. Chem. Phys.* **148**, 024501 (2018).
- [32] M. Cieřla and P. Kubala, Random sequential adsorption of cuboids, *J. Chem. Phys.* **149**, 194704 (2018).
- [33] M. Cieřla, Continuum random sequential adsorption of polymer on a flat and homogeneous surface, *Phys. Rev. E* **87**, 052401 (2013).
- [34] N. I. Lebovka, N. N. Karmazina, Y. Yu. Tarasevich, and V. V. Laptev, Random sequential adsorption of partially oriented linear  $k$ -mers on a square lattice, *Phys. Rev. E* **84**, 061603 (2011).
- [35] N. I. Lebovka, Y. Yu. Tarasevich, D. O. Dubinin, V. V. Laptev, and N. V. Vygornitskii, Jamming and percolation in generalized models of random sequential adsorption of linear  $k$ -mers on a square lattice, *Phys. Rev. E* **92**, 062116 (2015).
- [36] Jian-Sheng Wang and Ras B. Pandey, Kinetics and Jamming Coverage in A Random Sequential Adsorption of Polymer Chains, *Phys. Rev. Lett.* **77**, 1773 (1996).
- [37] B. Bonnier, Y. Leroyer, and E. Pommiers, Random sequential adsorption of line segments: Universal properties of mixtures in 1, 2, and 3D lattices, *J. Phys. I France* **2**, 379 (1992).
- [38] Y. Tarasevich and V. Cherkasova, Dimer percolation and jamming on simple cubic lattice, *Eur. Phys. J. B* **60**, 97 (2007).
- [39] D. J. Burridge, Random packing of lines in a lattice cube, *Phys. Rev. E* **81**, 031107 (2010).
- [40] G. D. García, F. O. Sanchez-Varretti, P. M. Centres, and A. J. Ramirez-Pastor, Random sequential adsorption of straight rigid rods on a simple cubic lattice, *Physica A: Stat. Mech. Appl.* **436**, 558 (2015).
- [41] J. Wang, Z. Zhou, W. Zhang, T. M. Garoni, and Y. Deng, Bond and site percolation in three dimensions, *Phys. Rev. E* **87**, 052107 (2013).
- [42] M. I. González, P. M. Centres, W. Lebrecht, and A. J. Ramirez-Pastor, Site-bond percolation on simple cubic lattices: Numerical simulation and analytical approach, *J. Stat. Mech.* (2016) 093210.
- [43] K. Malarz, Simple cubic random-site percolation thresholds for neighborhoods containing fourth-nearest neighbors, *Phys. Rev. E* **91**, 043301 (2015).
- [44] R. M. Ziff and S. Torquato, Percolation of disordered jammed sphere packings, *J. Phys. A: Math. Theor.* **50**, 085001 (2017).
- [45] J.-F. Thovert, V. V. Mourzenko, and P. M. Adler, Percolation in three-dimensional fracture networks for arbitrary size and shape distributions, *Phys. Rev. E* **95**, 042112 (2017).
- [46] S. Torquato, T. M. Truskett, and P. G. Debenedetti, Is Random Close Packing of Spheres Well Defined? *Phys. Rev. Lett.* **84**, 2064 (2000).
- [47] A. B. Harris and T. C. Lubensky, Connection between percolation and lattice animals, *Phys. Rev. B* **23**, 3591 (1981).
- [48] A. R. Conway and A. J. Guttmann, On two-dimensional percolation, *J. Phys. A: Math. Gen.* **28**, 891 (1995).
- [49] M. F. Sykes and M. Glen, Percolation processes in two dimensions. I. Low-density series expansions, *J. Phys. A: Math. Gen.* **9**, 87 (1976).
- [50] T. C. Lubensky and J. Isaacson, Statistics of lattice animals and dilute branched polymers, *Phys. Rev. A* **20**, 2130 (1979).
- [51] S. Flesia, D. S. Gaunt, C. E. Soteros, and S. G. Whittington, Statistics of collapsing lattice animals, *J. Phys. A: Math. Gen.* **27**, 5831 (1994).
- [52] W. F. Lunnon, Counting polyominoes, in *Computers in Number Theory*, edited by A. O. L. Atkin and B. J. Birch (Academic Press, San Diego, CA, 1971), pp. 347–372.

- [53] D. S. Gaunt, M. F. Sykes, and H. Ruskin, Percolation processes in D-dimensions, *J. Phys. A: Math. Gen.* **9**, 1899 (1976).
- [54] G. Aleksandrowicz and G. Barequet, Counting polycubes without the dimensionality curse, *Discrete Math.* **309**, 4576 (2009).
- [55] I. Jensen, Enumerations of lattice animals and trees, *J. Stat. Phys.* **102**, 865 (2001).
- [56] D. H. Redelmeier, Counting polyominoes: Yet another attack, *Discrete Math.* **36**, 191 (1981).
- [57] W. F. Lunnon, Symmetry of cubical and general polyominoes, in *Graph Theory and Computing*, edited by Ronald C. Read (Academic Press, San Diego, CA, 1972), pp. 101–108.
- [58] OEIS Foundation Inc., Sequence A000162, in The On-Line Encyclopedia of Integer Sequences, edited by N. J. A. Sloane (2019), <http://oeis.org/A000162>.
- [59] H. Goldstein, C. Pole, and J. Safko, *Classical Mechanics*, 3rd ed. (Addison Wesley, San Francisco, CA, 2002).
- [60] N. Ch. Karayiannis and M. Laso, Dense and Nearly Jammed Random Packings of Freely Jointed Chains of Tangent Hard Spheres, *Phys. Rev. Lett.* **100**, 050602 (2008).
- [61] N. Ch. Karayiannis and M. Laso, Monte Carlo scheme for generation and relaxation of dense and nearly jammed random structures of freely jointed hard-sphere chains, *Macromolecules* **41**, 1537 (2008).